Available online at www.sciencedirect.com
ScienceDirect
Mathematics and Computers in Simulation 73 (2006) 2–20
MATHEMATICS AND COMPUTERS IN SIMULATION
www.elsevier.com/locate/matcom

Three-phase immiscible displacement in heterogeneous petroleum reservoirs

E. Abreu[a,*], J. Douglas Jr. [b], F. Furtado[c], D. Marchesin[d], F. Pereira[a]

[a] *Departamento de Modelagem Computacional, Instituto Politécnico/UERJ, Caixa Postal 97282, Nova Friburgo 28601-970, RJ, Brazil*
[b] *Department of Mathematics, Purdue University, West Lafayette, IN 47907-1395, USA*
[c] *Department of Mathematics, University of Wyoming, Laramie, WY 82071-3036, USA*
[d] *Instituto Nacional de Matemática Pura e Aplicada, Estrada D. Castorina 110, Rio de Janeiro 22460-320, RJ, Brazil*

Available online 14 August 2006

Abstract

We describe a fractional-step numerical procedure for the simulation of immiscible three-phase flow in heterogeneous porous media that takes into account capillary pressure and apply it to indicate the existence of a so-called “transitional" wave in at least some multi-dimensional flows, thereby extending theoretical results for one-dimensional flows. The step procedure combines a second-order, conservative central difference scheme for a pertinent system of conservation laws modeling the convective transport of the fluid phases with locally conservative mixed finite elements for the associated parabolic and elliptic problems.

Keywords: Operator splitting; Mixed finite elements; Central difference scheme; Three-phase flow; Heterogeneous reservoirs

1. Introduction

In immiscible, incompressible three-phase flow in porous media for which advection dominates diffusive or capillary effects, the leading front caused by injection intended to move one or more of the phases toward a production point can split into a classical Buckley–Leverett shock followed by a new type of shock wave related to the existence of an elliptic region or an umbilic point for the system of nonlinear conservation laws describing the convective transport of the fluid phases. Unlike classical Buckley–Leverett fronts, this nonclassical “transitional” shock wave is very sensitive to the form of the parabolic (capillary) terms in the equations; see [31] and references therein. Thus, it is imperative that capillary pressure effects be modeled accurately in order to calculate physically correct transitional waves.

Transitional waves (also called undercompressive and intermediate waves) have been identified for flows in a linear domain [26,16,37,22,23] and for a number of other physical problems such as magneto-hydrodynamics, van der Waals gases and combustion. Recently [8] it was determined that transitional waves arise in lubrication flow.

The purposes of this work are to present an accurate numerical procedure for the simulation of three-phase flows including capillarity and to apply the technique to show the existence of transitional waves in multi-dimensional flows for some reasonable capillary pressure functions. The numerical procedure is validated in two ways; first, semi-analytic one-dimensional results [31] are closely reproduced computationally by the numerical method [1,2] and, second, a

* Corresponding author. Tel.: +55 22 2528 8545x303; fax: +55 22 2528 8536.
E-mail addresses: eabreu@iprj.uerj.br (E. Abreu).

0378-4754/$32.00 © 2006 IMACS. Published by Elsevier B.V. All rights reserved.
doi:10.1016/j.matcom.2006.06.018

numerical convergence study is presented for a two-dimensional reservoir having moderately inhomogeneous physical parameters. Then, we focus on two-dimensional problems arising from fractally heterogeneous geology. (We shall use the terminology of waterflooding in petroleum reservoirs—including calling the three fluids oil, water, and gas.) Our calculations verify that transitional waves are present in two-dimensional heterogenous reservoirs for at least some reasonable capillary pressure functions. To the authors' knowledge such results have not been reported previously in the literature.

Our new procedure is a two-level operator-splitting procedure with mixed finite element methods being used for the approximation of the parabolic problem for diffusion (capillarity) and the elliptic problem for the pressure and a Darcy velocity combined with a nonoscillatory, second-order, conservative central difference scheme to handle a system of nonlinear conservation laws describing advection. As announced above, the technique is designed to treat the numerical solution of three-phase, immiscible displacement problems in heterogeneous porous media; the numerical tests performed indicate that the two-dimensional simulator produces accurate approximations of the differential equations making up the model.

Different approaches for solving numerically the three-phase flow equations can be found in [7,9,10].

2. Three-phase flow

We consider two-dimensional, horizontal flow of three immiscible, incompressible fluid phases in a porous medium. For concreteness, the phases will be called gas, oil, and water and indicated by the subscripts g, o, and w, respectively. We assume that there are no internal sources or sinks. Compressibility, mass transfer between phases, and thermal and gravitational effects are neglected.

We assume that the three fluid phases saturate the pores; thus, with S_i denoting the saturation (local volume fraction) of phase i,

$$\sum_{i=\mathrm{g,o,w}} S_i = 1. \tag{1}$$

Consequently, any pair of saturations inside the triangle of saturations

$$\triangle := \{(S_i, S_j) :\ S_i, S_j \geq 0,\ S_i + S_j \leq 1,\ i \neq j\} \tag{2}$$

can be chosen to describe the state of the fluid. In our model we shall work with the saturations S_w and S_g of water and gas. First, let us derive the governing equations for our model.

The equations expressing conservation of mass of oil, water and gas are

$$\frac{\partial}{\partial t}(\phi S_i \rho_i) + \nabla\cdot(\rho_i \mathbf{v}_i) = 0, \quad i = \mathrm{o, w, g}, \tag{3}$$

respectively, where ϕ denotes the porosity of the porous medium. For the phase i, S_i denotes its saturation and ρ_i its density, and $\mathbf{v}_i$ is its volumetric rate of flow (or, Darcy velocity) and is given by the multiphase Darcy law [34,36,6]

$$\mathbf{v}_i = -K(\mathbf{x})\lambda_i \nabla p_i, \quad i = \mathrm{o, w, g}, \tag{4}$$

where $K(\mathbf{x})$ denotes absolute permeability of the porous medium; $\lambda_i \geq 0$ and p_i are the mobility and the pressure of phase i, respectively. The mobility is usually expressed as

$$\lambda_i = \frac{k_i}{\mu_i}, \tag{5}$$

the ratio of the relative permeability k_i and the viscosity μ_i of the phase i. Each relative permeability k_i depends on the saturation vector. Experimentally, k_i increases when S_i increases, and the relative permeabilities never vanish simultaneously. The porosity ϕ and the absolute permeability $K(\mathbf{x})$ are properties of the medium; we take the porosity to be constant and the permeability to be a function of position in the reservoir. If thermal effects and compressibility are neglected, μ_i and ρ_i are constant, and (3) can be rewritten in volumetric form:

$$\frac{\partial}{\partial t}(\phi S_i) + \nabla\cdot\mathbf{v}_i = 0, \quad i = \mathrm{o, w, g}, \tag{6}$$

Denote the capillary pressure between phase i and phase j, $i \neq j$, by

$$p_{ij} = p_i - p_j; \tag{7}$$

clearly, only two of the possible six capillary pressures are independent, since

$$p_{ij} = -p_{ji}, \quad \text{and} \quad p_{ik} = p_{ij} + p_{jk}. \tag{8}$$

An independent pair must be measured experimentally as a function of the saturation vector.

Define the total mobility λ and the fractional flow functions f_i by

$$\lambda = \sum_j \lambda_j \quad \text{and} \quad f_i = \frac{\lambda_i}{\lambda}. \tag{9}$$

Clearly, $\sum_j f_j = 1$. Let the total velocity (total volumetric flow rate) be given by

$$\mathbf{v} = \sum_j \mathbf{v}_j. \tag{10}$$

After a bit of algebraic manipulation, we can see that

$$\mathbf{v} f_i = -K\lambda_i \sum_j f_j \nabla p_j. \tag{11}$$

If we add and subtract $\mathbf{v}_i$ in the last equation and note that $\nabla p_i = (\sum_j f_j)\nabla p_i$, we see that

$$\mathbf{v}_i = \mathbf{v} f_i + K\lambda_i \sum_{j \neq i} f_j \nabla p_{ji}. \tag{12}$$

Therefore, by (6) and (12), the equations governing the flow are

$$\begin{aligned}
&\frac{\partial(\phi\, S_\mathrm{w})}{\partial t} + \nabla\cdot(\mathbf{v} f_\mathrm{w}) = \nabla\cdot[K\lambda_\mathrm{w}(f_\mathrm{g}\nabla p_\mathrm{wg} + f_\mathrm{o}\nabla p_\mathrm{wo})],\\
&\frac{\partial(\phi\, S_\mathrm{g})}{\partial t} + \nabla\cdot(\mathbf{v} f_\mathrm{g}) = \nabla\cdot[K\lambda_\mathrm{g}(f_\mathrm{w}\nabla p_\mathrm{gw} + f_\mathrm{o}\nabla p_\mathrm{go})],\\
&\frac{\partial(\phi\, S_\mathrm{o})}{\partial t} + \nabla\cdot(\mathbf{v} f_\mathrm{o}) = \nabla\cdot[K\lambda_\mathrm{o}(f_\mathrm{w}\nabla p_\mathrm{ow} + f_\mathrm{g}\nabla p_\mathrm{og})].
\end{aligned} \tag{13}$$

Any one of the Eq. (13) is redundant, and the system can be reduced to a two-component system. As a result of the redundancy in (13), one of its characteristic speeds is 0. The two other characteristic speeds are the same for any subsystem of two equations (see [32]).

As a consequence of the redundancy, the system can be written in the form of a pair of saturation equations and a Darcy pressure–velocity system. The Eq. (15a) results from adding the three equations in (13), and the derivation of (16) is facilitated by applying the relation $p_\mathrm{wg} = p_\mathrm{wo} + p_\mathrm{og}$. The governing equations then become as follows:

Saturation equations:

$$\frac{\partial(\phi S_\mathrm{w})}{\partial t} + \nabla\cdot(\mathbf{v} f_\mathrm{w}(S_\mathrm{w}, S_\mathrm{g})) = \nabla\cdot\mathbf{w}_\mathrm{w}, \tag{14a}$$

$$\frac{\partial(\phi S_\mathrm{g})}{\partial t} + \nabla\cdot(\mathbf{v} f_\mathrm{g}(S_\mathrm{w}, S_\mathrm{g})) = \nabla\cdot\mathbf{w}_\mathrm{g}, \tag{14b}$$

Pressure–velocity equations:

$$\nabla\cdot\mathbf{v} = 0, \tag{15a}$$

$$\mathbf{v} = -K(\mathbf{x})\lambda(S_\mathrm{w}, S_\mathrm{g})\nabla p_\mathrm{o} + \mathbf{v}_\mathrm{wo} + \mathbf{v}_\mathrm{go}. \tag{15b}$$

The flux terms $\mathbf{w}_\mathrm{w}$ and $\mathbf{w}_\mathrm{g}$ are given by

$$[\mathbf{w}_\mathrm{w}, \mathbf{w}_\mathrm{g}]^\mathrm{T} = K(\mathbf{x})\, B(S_\mathrm{w}, S_\mathrm{g}) \left[\nabla S_\mathrm{w}, \nabla S_\mathrm{g}\right]^\mathrm{T}. \tag{16}$$

Here, [**a**, **b**] denotes the 2×2 matrix with column vectors **a** and **b**, and $B = QP'$, where

$$Q(S_w, S_g) = \begin{bmatrix} \lambda_w(1 - f_w) & -\lambda_w f_g \\ -\lambda_g f_w & \lambda_g(1 - f_g) \end{bmatrix}, \qquad P'(S_w, S_g) = \begin{bmatrix} \dfrac{\partial p_{wo}}{\partial S_w} & \dfrac{\partial p_{wo}}{\partial S_g} \\ \dfrac{\partial p_{go}}{\partial S_w} & \dfrac{\partial p_{go}}{\partial S_g} \end{bmatrix}. \tag{17}$$

In the above, the correction velocities $\mathbf{v}_{wo}$ and $\mathbf{v}_{go}$ are defined by

$$\mathbf{v}_{ij} = -K(\mathbf{x})\lambda_i(S_w, S_g)\nabla p_{ij}. \tag{18}$$

The diffusive (capillary) term is represented by the right-hand side of the system (14). For our model one can verify that this term is strictly parabolic in the interior of the saturation triangle $\triangle$ [5].

Boundary and initial conditions for (14)–(18) must be imposed to complete the definition of the mathematical model; in particular, S_w and S_g must be specified at the initial time $t = 0$. The boundary conditions will be introduced in the description of the operator splitting for the numerical method; the computed fluid flow, in two space dimensions reported here, are defined in a bounded two-dimensional reservoir $\Omega = [0, X] \times [0, Y]$.

3. A fractional-step procedure

We employ a two-level operator-splitting procedure for the numerical solution of the three-phase flow system in which we first split the pressure–velocity calculation from the saturation calculation and then split the saturation calculation into advection and diffusion. The splitting allows time steps for the pressure–velocity calculation that are longer than those for the diffusive calculation, which are in turn longer than those for advection. Thus, we introduce three time steps: Δt_t for the solution of the hyperbolic problem for the advection, Δt_d for the diffusive calculation and Δt_p for the pressure–velocity calculation:

$$\Delta t_p = i_1 \Delta t_d = i_1 i_2 \Delta t_t, \tag{19}$$

where i_1 and i_2 are positive integers, so that $\Delta t_p \geq \Delta t_d \geq \Delta t_t$. Let

$$t^m = m\Delta t_p, \qquad t_n = n\Delta t_d \quad \text{and} \quad t_{n,\kappa} = t_n + \kappa \Delta t_t, \quad 0 \leq \kappa \leq i_2, \tag{20}$$

so that $t_{n,i_2} = t_{n+1}$. Then, given a generic function z, denote its values at times t^m, t_n, and $t_{n,\kappa}$ by z^m, z_n, and $z_{n,\kappa}$.

In practice, variable time steps are always useful, especially for the advection micro-steps subject dynamically to a CFL condition. To simplify the description of the operator splitting, assume each time step to have a single value.

The oil pressure (and Darcy velocity) will be approximated at times t^m, $m = 0, 1, 2, \ldots$. The saturations, S_w and S_g, will be approximated at times t_n, $n = 1, 2, \ldots$; recall that they were specified at $t = 0$. In addition, there will be values for the saturation computed at intermediate times $t_{n,\kappa}$ for $t_n < t_{n,\kappa} \leq t_{n+1}$ that take into account the advective transport of the water and gas but not the diffusive effects. The algorithm will be detailed below.

The initial conditions S_w and S_g at $t = 0$ allow the calculation of $\{p_o^0, \mathbf{v}^0\}$. The following is the fractional step algorithm associated with the differential form of three-phase model that should be followed until the final simulation time is reached. After this, the discretization will be taken up in detail.

3.1. First level

(1) Given $S_w^m(\mathbf{x})$ and $S_g^m(\mathbf{x})$, $m \geq 0$, determine $\{p_o^m, \mathbf{v}^m\}$ by (15)–(18), subject to the boundaries conditions

$$\begin{aligned} &\mathbf{v} \cdot \boldsymbol{\nu} = -q, \quad \text{for } x = 0, \quad y \in [0, Y], \\ &\mathbf{v} \cdot \boldsymbol{\nu} = q, \quad \text{for } x = X, \quad y \in [0, Y], \\ &\mathbf{v} \cdot \boldsymbol{\nu} = 0, \quad \text{for } y = 0, Y, \ x \in [0, X], \end{aligned} \tag{21}$$

where $\boldsymbol{\nu}$ is the unit outer normal vector to $\partial\Omega$.

(2) For $t^m < t \leq t^{m+1}$, solve the advection–diffusion system (14) with the initial conditions $S_w(\mathbf{x}, t^m) = S_w^m(\mathbf{x})$ and $S_g(\mathbf{x}, t^m) = S_g^m(\mathbf{x})$; $S_w^m(\mathbf{x})$ and $S_g^m(\mathbf{x})$ are evaluated as the final values of the calculation in $[t^{m-1}, t^m]$ for $m > 0$ or the initial saturations for $m = 0$.

3.2. Second level

(1) Let $t_{n_1} = t^m$ and assume that $\{p_o,\ \mathbf{v},\ S_w,\ S_g\}$ are known for $t \le t_{n_1}$.
(2) For $n = n_1, \ldots, n_2 = n_1 + (i_1 - 1)$:
   (a) For $\kappa = 0, \ldots, (i_2 - 1)$ and $t \in [t_{n,\kappa}, t_{n,\kappa+1}]$ solve the advection system given by (for notational convenience, $s_i^{n,\kappa}$ is replaced by s_i^κ below)

$$\frac{\partial(\phi\, s_i^\kappa)}{\partial t} + \nabla\cdot(\mathbf{E}(t_{n,\kappa}, \mathbf{v})\, f_i(s_w^\kappa, s_g^\kappa)) = 0, \quad i = w, g, \tag{22}$$

   where

$$s_i^\kappa(\mathbf{x}, t_{n,\kappa}) = \begin{cases} S_i(\mathbf{x}, t_n), & \kappa = 0 \\ s_i^{\kappa-1}(\mathbf{x}, t_{n,\kappa}), & \kappa = 1, \ldots, i_2 - 1, \end{cases}, \quad i = w, g \tag{23}$$

   and $\mathbf{E}(t_{n,\kappa}, \mathbf{v})$ indicates a linear extrapolation operator; it extrapolates to time $t_{n,\kappa}$ the velocity fields $\mathbf{v}^{m-1}$ and $\mathbf{v}^m$.
   (b) Set $\bar{S}_i(\mathbf{x}, t_n) = s_i^{i_2-1}(\mathbf{x}, t_{n,i_2}), \quad i = w, g.$
   (c) Compute the diffusive effects on $[t_n, t_{n+1}]$ by solving the system

$$\frac{\partial(\phi\, S_i)}{\partial t} - \nabla\cdot\mathbf{w}_i = 0, \quad i = w, g, \tag{24}$$

   with boundary conditions

$$\mathbf{w}_i \cdot \boldsymbol{\nu} = 0, \quad i = w, g,\ \mathbf{x} \in \partial\Omega, \tag{25}$$

   and initial conditions

$$S_i(\mathbf{x}, t_n) = \bar{S}_i(\mathbf{x}, t_n), \quad i = w, g. \tag{26}$$

Remark. The division of the interval $[t_n, t_{n+1}]$ into microsteps of length Δt_t is artificial in the differential case described above, but the division is desirable and often necessary after the full discretization of the advection equations is introduced.

(3) Set $S_i^{m+1}(\mathbf{x}) = S_i(\mathbf{x}, t_{n_2+1}), \quad i = w, g.$

4. Approximation by mixed finite elements

We shall use a singly-indexed notation for the rectangles in the partition $\{\Omega_j\}$ of Ω. Let $\{\Omega_j,\ j = 1, \ldots, M\}$ be a uniform partition of Ω into cells of size $h \times h$: $\bar{\Omega} = \cup_{j=1}^M \bar{\Omega}_j$; $\Omega_j \cap \Omega_k = \emptyset,\ j \ne k$. Let $\Gamma = \partial\Omega,\ \Gamma_j = \Gamma \cap \partial\Omega_j,\ \Gamma_{jk} = \Gamma_{kj} = \partial\Omega_j \cap \partial\Omega_k$.

4.1. Pressure–velocity equations

We now describe in detail Step (1) of Section 3.1. Assume that the saturations $\{S_w, S_g\}$ and their fluxes $\{\mathbf{w}_w, \mathbf{w}_g\}$ are known. Then, the phase velocity corrections $\mathbf{v}_{wo}$ and $\mathbf{v}_{go}$ can be calculated using $\{\mathbf{w}_w, \mathbf{w}_g\}$ as described below. Their sum defines a source term q_B. Then, the auxiliary problem (27) defined below for the pair $(p_o, \mathbf{u})$ must be solved. Finally, the total velocity can be recovered from (15b).

4.1.1. An auxiliary problem

Define the auxiliary problem for $(p_o, \mathbf{u})$:

$$\mathbf{u} = -K(\mathbf{x})\lambda(S_w, S_g)\nabla p_o, \tag{27a}$$

$$\nabla\cdot\mathbf{u} = -\nabla\cdot(\mathbf{v}_{wo} + \mathbf{v}_{go}) \equiv q_B, \tag{27b}$$

subject to the boundary conditions (21).

Note that, by (16), the diffusive fluxes $\mathbf{w}_w$ and $\mathbf{w}_g$ can be expressed in terms of the correction velocities $\mathbf{v}_{wo}$ and $\mathbf{v}_{go}$:

$$\mathbf{w}_w = (f_w - 1)\mathbf{v}_{wo} + f_w\mathbf{v}_{go}, \qquad \mathbf{w}_g = f_g\mathbf{v}_{wo} + (f_g - 1)\mathbf{v}_{go}. \tag{28}$$

Next, express the correction velocities in (28) as functions of the the diffusive fluxes:

$$\mathbf{v}_{wo} = \frac{(f_g - 1)}{f_o}\mathbf{w}_w - \frac{f_w}{f_o}\mathbf{w}_g, \qquad \mathbf{v}_{go} = -\frac{f_g}{f_o}\mathbf{w}_w + \frac{(f_w - 1)}{f_o}\mathbf{w}_g. \tag{29}$$

Adding the equations in (29) gives

$$\mathbf{v}_{wo} + \mathbf{v}_{go} = -\frac{\lambda}{\lambda_o}(\mathbf{w}_w + \mathbf{w}_g). \tag{30}$$

Thus,

$$q_B = \nabla\cdot\left(\frac{\lambda}{\lambda_o}(\mathbf{w}_w + \mathbf{w}_g)\right), \tag{31}$$

with boundary conditions specified in (25).

Observe that (25), (31), and the divergence theorem imply that

$$\int_\Omega q_B \, dx = 0. \tag{32}$$

4.1.2. Numerical solution of the auxiliary problem

We shall approximate the solution of (27) - subject to the boundary conditions (21) - by applying the mixed finite element method based on the space $\mathbf{W}^h \times \mathbf{V}^h$ given by the lowest index Raviart–Thomas space [35] over rectangles.

The natural degrees of freedom on the element Ω_j are the (constant) value p_{o_j} of the pressure over Ω_j, which can be interpreted as the value at the center of the element, and the four (constant) values $u_{j\beta}$, $\beta \in \{L, R, B, T\} = \{\text{left, right, bottom, top}\}$, of the outward normal component of $\mathbf{u}$ across the edges of the element. Hybridize [3,12,13] the mixed method by introducing Lagrange multipliers $\ell_{o_{j\beta}}$, $\beta = L, R, B, T$, for the oil pressure on Γ_{jk}; $\ell_{o_{j\beta}}$ is constant on each edge. We shall assume the porosity and the absolute permeability to be constant on each element and the capillary pressure and relative permeability functions to be independent of position. Thus, the coefficients are constant on each Ω_j with respect to the space variable.

Then, the discrete form of (27b) can be written as

$$u_{jL} + u_{jR} + u_{jB} + u_{jT} = q_{B_j}h; \tag{33}$$

here, q_{B_j} should be evaluated using (31) and the divergence theorem. A particularly simple discrete form of (27a) is obtained by applying a trapezoidal rule for the evaluation of the pertinent integrals (see [13]):

$$u_{j\beta} - \frac{2}{h}K_j\lambda_{j\beta}(p_{o_j} - \ell_{o_{j\beta}}) = 0, \quad \beta = L, R, B, T, \tag{34}$$

where the total mobility function $\lambda_{j\beta}$ is defined through the Lagrange multipliers for the saturations on the interface β (see Section 4.2).

The linear algebra system resulting from the discretized equations can be solved by a preconditioned conjugate gradient procedure (PCG) or by a multigrid procedure [13].

4.2. Diffusion system

We discuss a numerical procedure that we employ for the solution of the diffusive system (24)–(26) which combines domain decomposition with an implicit time discretization in the construction of an efficient iterative method.

We consider an element-by-element domain decomposition; in addition to requiring that the pairs $(S_{w_j}, \mathbf{w}_{w_j})$ and $(S_{g_j}, \mathbf{w}_{g_j})$ (where $S_{i_j} = S_i|_{\Omega_j}$, $i = w, g$, etc.) be a solution of (24)–(26) for $\mathbf{x} \in \Omega_j$, $j = 1, \ldots, M$; it is necessary to

impose the consistency conditions,

$$\begin{aligned} &S_{\mathrm{w}_j} = S_{\mathrm{w}_k}, \quad \mathbf{x} \in \Gamma_{jk}, \\ &\mathbf{w}_{\mathrm{w}_{jk}} \cdot \boldsymbol{\nu}_j + \mathbf{w}_{\mathrm{w}_{kj}} \cdot \boldsymbol{\nu}_k = 0, \quad \mathbf{x} \in \Gamma_{jk}, \end{aligned} \tag{35}$$

and

$$\begin{aligned} &S_{\mathrm{g}_j} = S_{\mathrm{g}_k}, \quad \mathbf{x} \in \Gamma_{jk}, \\ &\mathbf{w}_{\mathrm{g}_{jk}} \cdot \boldsymbol{\nu}_j + \mathbf{w}_{\mathrm{g}_{kj}} \cdot \boldsymbol{\nu}_k = 0, \quad \mathbf{x} \in \Gamma_{jk}, \end{aligned} \tag{36}$$

where $\boldsymbol{\nu}_j$ is a outward normal unit vector of Ω_j.

In order to define an iterative method to solve the above problem, it will be convenient to replace (35) and (36) by equivalent Robin transmission boundary conditions [14]. These consistency conditions are given by

$$-\chi_{\mathrm{w}_{jk}} \mathbf{w}_{\mathrm{w}_j} \cdot \boldsymbol{\nu}_{j_j} + S_{\mathrm{w}_j} = \chi_{\mathrm{w}_{jk}} \mathbf{w}_{\mathrm{w}_k} \cdot \boldsymbol{\nu}_{j_k} + S_{\mathrm{w}_k}, \quad \mathbf{x} \in \Gamma_{jk} \subset \partial\Omega_j, \tag{37}$$

$$-\chi_{\mathrm{w}_{kj}} \mathbf{w}_{\mathrm{w}_k} \cdot \boldsymbol{\nu}_{j_k} + S_{\mathrm{w}_k} = \chi_{\mathrm{w}_{kj}} \mathbf{w}_{\mathrm{w}_j} \cdot \boldsymbol{\nu}_{j_j} + S_{\mathrm{w}_j}, \quad \mathbf{x} \in \Gamma_{kj} \subset \partial\Omega_k, \tag{38}$$

$$-\chi_{\mathrm{g}_{jk}} \mathbf{w}_{\mathrm{g}_j} \cdot \boldsymbol{\nu}_{j_j} + S_{\mathrm{g}_j} = \chi_{\mathrm{g}_{jk}} \mathbf{w}_{\mathrm{g}_k} \cdot \boldsymbol{\nu}_{j_k} + S_{\mathrm{g}_k}, \quad \mathbf{x} \in \Gamma_{jk} \subset \partial\Omega_j, \tag{39}$$

$$-\chi_{\mathrm{g}_{kj}} \mathbf{w}_{\mathrm{g}_k} \cdot \boldsymbol{\nu}_{j_k} + S_{\mathrm{g}_k} = \chi_{\mathrm{g}_{kj}} \mathbf{w}_{\mathrm{g}_j} \cdot \boldsymbol{\nu}_{j_j} + S_{\mathrm{g}_j}, \quad \mathbf{x} \in \Gamma_{kj} \subset \partial\Omega_k, \tag{40}$$

where $\chi_{\mathrm{w}_{jk}}$ and $\chi_{\mathrm{g}_{jk}}$ are positive functions on Γ_{jk} (see [1,14]).

We consider the lowest index Raviart–Thomas space [35] over Ω_j to approximate the pairs $(S_{\mathrm{w}}, \mathbf{w}_{\mathrm{w}})$ and $(S_{\mathrm{g}}, \mathbf{w}_{\mathrm{g}})$. The degrees of freedom on an element Ω_j are the values S_{w_j} and S_{g_j} and the two values $w_{\mathrm{w}_{j\beta}}$ and $w_{\mathrm{g}_{j\beta}}$, $\beta = \mathrm{L}, \mathrm{R}, \mathrm{B}, \mathrm{T}$, of the diffusive fluxes across the edge of the elements. We shall also introduce the Lagrange multipliers ℓ_{w_β} and ℓ_{g_β}, $\beta = \mathrm{L}, \mathrm{R}, \mathrm{B}, \mathrm{T}$, for the water and gas saturations, respectively, on Γ_{jk}; these multipliers are constant on each edge.

So, the discrete form of (24) can be written as (see [1,13]):

$$\phi \left(\frac{S_{\mathrm{w}_j} - \bar{S}_{\mathrm{w}_j}}{\Delta t_{\mathrm{d}}} \right) - \frac{1}{h} \left(w_{\mathrm{w}_{j_{\mathrm{U}}}} + w_{\mathrm{w}_{j_{\mathrm{R}}}} + w_{\mathrm{w}_{j_{\mathrm{D}}}} + w_{\mathrm{w}_{j_{\mathrm{L}}}} \right) = 0, \tag{41}$$

$$w_{\mathrm{w}_{j\beta}} B^{-1}_{11_\beta} + w_{\mathrm{g}_{j\beta}} B^{-1}_{12_\beta} = \frac{2}{h} (S_{\mathrm{w}_j} - \ell_{\mathrm{w}_{j\beta}}), \quad \beta = \mathrm{L}, \mathrm{R}, \mathrm{B}, \mathrm{T}, \tag{42}$$

$$\phi \left(\frac{S_{\mathrm{g}_j} - \bar{S}_{\mathrm{g}_j}}{\Delta t_{\mathrm{d}}} \right) - \frac{1}{h} \left(w_{\mathrm{g}_{j_{\mathrm{U}}}} + w_{\mathrm{g}_{j_{\mathrm{R}}}} + w_{\mathrm{g}_{j_{\mathrm{D}}}} + w_{\mathrm{g}_{j_{\mathrm{L}}}} \right) = 0, \tag{43}$$

$$w_{\mathrm{w}_{j\beta}} B^{-1}_{21_\beta} + w_{\mathrm{g}_{j\beta}} B^{-1}_{22_\beta} = \frac{2}{h} (S_{\mathrm{g}_j} - \ell_{\mathrm{g}_{j\beta}}), \quad \beta = \mathrm{L}, \mathrm{R}, \mathrm{B}, \mathrm{T}, \tag{44}$$

where $B^{-1}_{ij_\beta}$ are the entries of the inverse matrix $B^{-1}(\ell_{\mathrm{w}_\beta}, \ell_{\mathrm{g}_\beta})$. Here also a trapezoidal rule is used for the evaluation of the pertinent integrals in the derivation of Eqs. (42) and (44).

Define an iterative scheme for the solution of system (24) by applying (37), (38) to (42) and (39), (40) to (44) to express all Lagrange multipliers in terms of Lagrange multipliers and fluxes associated with adjacent elements. This scheme, developed in [1] (see also [13]), is a natural extension for parabolic systems of the procedure introduced in [14] for scalar elliptic and parabolic problems.

5. Approximation by a central difference scheme

We shall discuss the high-resolution finite difference scheme, introduced by Nessyahu and Tadmor (NT) [33], that we employ for the solution of the nonlinear advection system (22)–(23). This scheme can be viewed as an extension of the celebrated first-order Lax–Friedrichs scheme into a second-order scheme. Its two main ingredients are a non-oscillatory, piecewise bilinear reconstruction of the solution point-values from their given cell averages and central differencing based on the *staggered* reconstructed averages. The piecewise bilinear reconstruction reduces the excessive dissipation of the Lax–Friedrichs scheme and, like upwind schemes, the scheme uses nonlinear limiters to guarantee the overall nonoscillatory nature of the approximate solution. The central differencing, unlike upwind differencing, bypasses the

need for Riemann solvers, yielding simplicity, avoiding dimensional splitting in multi-dimensional problems. Central differencing also allows for the extension of the scheme to hyperbolic systems by componentwise application of the scalar framework.

5.1. The scalar framework in two space dimensions

Consider the model of hyperbolic conservation law,

$$\frac{\partial s}{\partial t} + \frac{\partial (f(s)v_x)}{\partial x} + \frac{\partial (f(s)v_y)}{\partial y} = 0. \tag{45}$$

Here $v_x \equiv v_x(x, y, t)$ and $v_y \equiv v_y(x, y, t)$ denote the x and y components of the velocity field $\mathbf{v}$.

Consider the cell averages,

$$s_{j,k}(t) \equiv \frac{1}{h^2} \int_{x_{j-(1/2)}}^{x_{j+(1/2)}} \int_{y_{k-(1/2)}}^{y_{k+(1/2)}} s(x, y, t)\, \mathrm{d}x\, \mathrm{d}y. \tag{46}$$

To approximate a solution to (45), at each time level, we start with a piecewise bilinear approximation of the cell averages (46), defined by

$$P_{j,k}(x, y, t_{n,\kappa}) = s_{j,k}(t_{n,\kappa}) + (x - x_j)\frac{1}{h}s'_{j,k}(t_{n,\kappa}) + (y - y_k)\frac{1}{h}\hat{s}_{j,k}(t_{n,\kappa}),$$
$$x_{j-(1/2)} \le x \le x_{j+(1/2)},\ y_{k-(1/2)} \le y \le y_{k+(1/2)}. \tag{47}$$

In Eq. (47),

$$\frac{1}{h}s'_{j,k}(t_{n,\kappa}) = \frac{\partial}{\partial x}s(x_j, y_k, t_{n,\kappa}) + O(h)s_x \tag{48}$$

and

$$\frac{1}{h}\hat{s}_{j,k}(t_{n,\kappa}) = \frac{\partial}{\partial y}s(x_j, y_k, t_{n,\kappa}) + O(h)s_y \tag{49}$$

denote the discrete slopes in the x and y directions. We shall discuss later the form of such discrete slopes.

The reconstruction (47) retains conservation, i.e.:

$$\frac{1}{h^2} \int_{x_{j-(1/2)}}^{x_{j+(1/2)}} \int_{y_{k-(1/2)}}^{y_{k+(1/2)}} P(x, y, t)\, \mathrm{d}x\, \mathrm{d}y = s_{j,k}(t). \tag{50}$$

The time evolution of this reconstruction is based on the integration of the conservation law (45) over staggered volumes $I_{j+(1/2),k+(1/2)} \times [t_{n,\kappa}, t_{n,\kappa} + \Delta t_t]$ (dashed grid in Fig. 1). The piecewise bilinear approximation of the cell averages is evolved in time, and then the result is projected on the staggered cells (dashed grid in Fig. 1) $I_{j+(1/2),k+(1/2)}$ to yield new cell averages.

The solution in the staggered grid obtained by the time evolution can be expressed as:

$$s_{j+(1/2),k+(1/2)}(t_{n,\kappa} + \Delta t_t) = \bar{s}(x, y, t_{n,\kappa} + \Delta t_t) \equiv \frac{1}{h^2} \int_{x_j}^{x_{j+1}} \int_{y_k}^{y_{k+1}} s(x, y, t_{n,\kappa} + \Delta t_t)\, \mathrm{d}x\, \mathrm{d}y,$$
$$x_j \le x \le x_{j+1},\ y_k \le y \le y_{k+1}. \tag{51}$$

By the conservation law (45), the integral in (51) equals

$$\begin{aligned} &s_{j+(1/2),k+(1/2)}(t_{n,\kappa} + \Delta t_t) \\ &= \frac{1}{h^2} \int_{x_j}^{x_{j+(1/2)}} \int_{y_k}^{y_{k+(1/2)}} P_{j,k}(x, y, t_{n,\kappa})\, \mathrm{d}x\, \mathrm{d}y + \frac{1}{h^2} \int_{x_j}^{x_{j+(1/2)}} \int_{y_{k+(1/2)}}^{y_{k+1}} P_{j,k+1}(x, y, t_{n,\kappa})\, \mathrm{d}x\, \mathrm{d}y \\ &+ \frac{1}{h^2} \int_{x_{j+(1/2)}}^{x_{j+1}} \int_{y_k}^{y_{k+(1/2)}} P_{j+1,k}(x, y, t_{n,\kappa})\, \mathrm{d}x\, \mathrm{d}y + \frac{1}{h^2} \int_{x_{j+(1/2)}}^{x_{j+1}} \int_{y_{k+(1/2)}}^{y_{k+1}} P_{j+1,k+1}(x, y, t_{n,\kappa})\, \mathrm{d}x\, \mathrm{d}y \end{aligned}$$

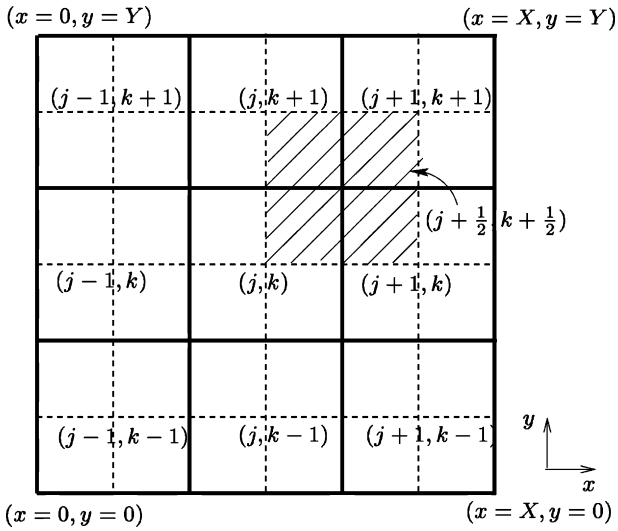

Fig. 1. Evolution step for the two-dimensional central scheme.

$$-\frac{1}{h^2}\left[\int_{t_{n,\kappa}}^{t_{n,\kappa}+\Delta t_t}\int_{x_j}^{x_{j+1}}(v_x(x_{j+1},y,t)f(s(x_{j+1},y,t))-v_x(x_j,y,t)f(s(x_j,y,t)))\,\mathrm{d}x\,\mathrm{d}t\right]$$
$$-\frac{1}{h^2}\left[\int_{t_{n,\kappa}}^{t_{n,\kappa}+\Delta t_t}\int_{y_k}^{y_{k+1}}(v_y(x,y_{k+1},t)f(s(x,y_{k+1},t))-v_y(x,y_k,t)f(s(x,y_k,t)))\,\mathrm{d}x\,\mathrm{d}t\right]. \tag{52}$$

The first four bilinear integrands on the RHS of (52) can be integrated exactly. The remaining integrals on the RHS of (52) involve approximations for the fluxes through the sides of the staggered volume. It is here that the benefit of staggering manifests itself: these fluxes are smooth at the vertices of the cell defining the integration volume, since these vertices are located at the centers of non-staggered cells, away from the jump discontinuities along the edges (see Fig. 1). This facilitates the construction of second-order approximations. The spatial integrals in both the x and y directions are approximated by the second-order trapezoid quadrature rule and the temporal integrals are approximated by the midpoint quadrature rule. Then, the resulting new approximate cell averages for the interior elements take the following form ($\alpha \equiv \Delta t_t/h$ and $s^{t_{n,\kappa}+\Delta t_t}_{j+(1/2),k+(1/2)} = s_{j+(1/2),k+(1/2)}(t_{n,\kappa}+\Delta t_t)$):

$$\begin{aligned}
s^{t_{n,\kappa}+\Delta t_t}_{j+(1/2),k+(1/2)} &= \tfrac{1}{4}(s^{t_{n,\kappa}}_{j,k}+s^{t_{n,\kappa}}_{j,k+1}+s^{t_{n,\kappa}}_{j+1,k}+s^{t_{n,\kappa}}_{j+1,k+1})+\tfrac{1}{16}(s'^{t_{n,\kappa}}_{j,k}+s'^{t_{n,\kappa}}_{j,k+1}-s'^{t_{n,\kappa}}_{j+1,k}\\
&\quad -s'^{t_{n,\kappa}}_{j+1,k+1}+s'^{t_{n,\kappa}}_{j,k}-s'^{t_{n,\kappa}}_{j,k+1}+s'^{t_{n,\kappa}}_{j+1,k}-s'^{t_{n,\kappa}}_{j+1,k+1})\\
&\quad +\tfrac{1}{2}\alpha\left[v_x{}^{t_{n,\kappa}+(\Delta t_t/2)}_{j,k}f(s^{t_{n,\kappa}+(\Delta t_t/2)}_{j,k})+v_x{}^{t_{n,\kappa}+(\Delta t_t/2)}_{j,k+1}f(s^{t_{n,\kappa}+(\Delta t_t/2)}_{j,k+1})\right.\\
&\quad \left.-v_x{}^{t_{n,\kappa}+(\Delta t_t/2)}_{j+1,k}f(s^{t_{n,\kappa}+(\Delta t_t/2)}_{j+1,k})-v_x{}^{t_{n,\kappa}+(\Delta t_t/2)}_{j+1,k+1}f(s^{t_{n,\kappa}+(\Delta t_t/2)}_{j+1,k+1})\right]\\
&\quad +\tfrac{1}{2}\alpha\left[v_y{}^{t_{n,\kappa}+(\Delta t_t/2)}_{j,k}f(s^{t_{n,\kappa}+(\Delta t_t/2)}_{j,k})+v_y{}^{t_{n,\kappa}+(\Delta t_t/2)}_{j+1,k}f(s^{t_{n,\kappa}+(\Delta t_t/2)}_{j+1,k})\right.\\
&\quad \left.-v_y{}^{t_{n,\kappa}+(\Delta t_t/2)}_{j,k+1}f(s^{t_{n,\kappa}+(\Delta t_t/2)}_{j,k+1})-v_y{}^{t_{n,\kappa}+(\Delta t_t/2)}_{j+1,k+1}f(s^{t_{n,\kappa}+(\Delta t_t/2)}_{j+1,k+1})\right].
\end{aligned} \tag{53}$$

The approximation of the fluxes in (53) makes use of the midpoint values in time, $s^{t_{n,\kappa}+(\Delta t_t/2)}_{j,k} \sim s(x_j, y_k, t_{n,\kappa}+(\Delta t_t/2))$, as a predictor step. Since these mid-values are bounded away from the jump discontinuities along the edges, we may use a Taylor expansion and the conservation law (45) to evaluate $s_{j,k}(t_{n,\kappa}+(\Delta t_t/2))$. In view of the hyperbolic conservation

law (45) we can write

$$\frac{\partial s}{\partial t} = -\nabla \cdot (\mathbf{v} f(s)). \tag{54}$$

Note that by the chain rule the relation

$$\nabla \cdot (\mathbf{v} f(s)) = f(s)(\nabla \cdot \mathbf{v}) + \mathbf{v} \cdot \nabla f(s) \tag{55}$$

holds. Then,

$$\frac{\partial s}{\partial t} = -(f(s)(\nabla \cdot \mathbf{v}) + \mathbf{v} \cdot \nabla f(s)). \tag{56}$$

In our application we have $\nabla \cdot \mathbf{v} = 0$ (see Eq. (15a)). Then, Eq. (56) reduces to

$$\frac{\partial s}{\partial t} = -(\mathbf{v} \cdot \nabla f(s)) = -\left(v_x \frac{\partial f(s)}{\partial x} + v_y \frac{\partial f(s)}{\partial y} \right). \tag{57}$$

By Taylor expansion and the conservation law (45) we can use

$$s_{j,k}^{t_{n,\kappa}+(\Delta t/2)} = s_{j,k}^{t_{n,\kappa}} - \frac{1}{2} \left(v_{x\,j,k}^{t_{n,\kappa}} \frac{1}{h} f_{j,k}^{\prime t_{n,\kappa}} + v_{y\,j,k}^{t_{n,\kappa}} \frac{1}{h} \grave{f}_{j,k}^{t_{n,\kappa}} \right) \tag{58}$$

to approximate the midpoint values $s_{j,k}^{t_{n,\kappa}+(\Delta t_{\mathrm{t}}/2)} \sim s(x_j, y_k, t_{n,\kappa} + (\Delta t_{\mathrm{t}}/2))$. In Eq. (58),

$$\frac{1}{h} f'_{j,k}(t_{n,\kappa}) = \frac{\partial}{\partial x} f(s(x_j, y_k, t_{n,\kappa})) + O(h) \tag{59}$$

and

$$\frac{1}{h} \grave{f}_{j,k}(t_{n,\kappa}) = \frac{\partial}{\partial y} f(s(x_j, y_k, t_{n,\kappa})) + O(h) \tag{60}$$

are the discrete fluxes in the x and y directions, respectively; their specification will be discussed later.

The approximations (48), (49), (59) and (60) are required to produce a second-order scheme for the approximation of (45) (see [33]). To avoid oscillations, it is essential to reconstruct these discrete derivatives with built-in nonlinear limiters [33]. We note that no (approximate) Riemann solvers are involved and the nonoscillatory behavior of the scheme hinges on the reconstructed discrete slopes, as described above.

In our sequential scheme, when solving for the saturation in time, the total velocity $\mathbf{v}$ is given by the solution of the velocity–pressure Eqs. (15a) and (15b). Recall that the solution of the pressure equation utilizes the lowest order Raviart–Thomas mixed finite element method. Thus, the computed total velocity $\mathbf{v}$ is discontinuous at the vertices of the original non-staggered grid cells. This constitutes a problem for the staggered scheme (53), which requires the values of the total velocity $\mathbf{v}$ at these vertices at every other time step. To avoid this difficulty we employ the non-staggered version of the NT scheme.

To turn the staggered scheme (53) into a non-staggered scheme, we reaverage reconstructed values of the underlying staggered scheme, thus recovering the cell averages of the central scheme over the original non-staggered grid cells. First we reconstruct a piecewise bilinear interpolant at the time step $t_{n,\kappa} + \Delta t_{\mathrm{t}}$

$$\begin{aligned} P_{j+(1/2),k+(1/2)}(x, y, t_{n,\kappa}) = {} & s_{j+(1/2),k+(1/2)}(t_{n,\kappa}) + (x - x_{j+(1/2)}) \frac{1}{h} s'_{j+(1/2),k+(1/2)}(t_{n,\kappa}) \\ & + (y - y_{k+(1/2)}) \frac{1}{h} \grave{s}_{j+(1/2),k+(1/2)}(t_{n,\kappa}), \quad x_j \le x \le x_{j+1},\ y_k \le y \le y_{k+1}, \end{aligned} \tag{61}$$

as in (47), through the staggered cell averages given by (53), and reaveraged it over the original grid cells, giving the following non-staggered scheme:

$$\begin{aligned} s_{j,k}^{t_{n,\kappa}+\Delta t_{\mathrm{t}}} = {} & \tfrac{1}{4} (s_{j-(1/2),k-(1/2)}^{t_{n,\kappa}+\Delta t_{\mathrm{t}}} + s_{j-(1/2),k+(1/2)}^{t_{n,\kappa}+\Delta t_{\mathrm{t}}} + s_{j+(1/2),k-(1/2)}^{t_{n,\kappa}+\Delta t_{\mathrm{t}}} + s_{j+(1/2),k+(1/2)}^{t_{n,\kappa}+\Delta t_{\mathrm{t}}}) \\ & + \tfrac{1}{16} (s_{j-(1/2),k-(1/2)}^{\prime t_{n,\kappa}+\Delta t_{\mathrm{t}}} + s_{j-(1/2),k+(1/2)}^{\prime t_{n,\kappa}+\Delta t_{\mathrm{t}}} - s_{j+(1/2),k-(1/2)}^{\prime t_{n,\kappa}+\Delta t_{\mathrm{t}}} - s_{j+(1/2),k+(1/2)}^{\prime t_{n,\kappa}+\Delta t_{\mathrm{t}}}) + \tfrac{1}{16} (\grave{s}_{j-(1/2),k-(1/2)}^{t_{n,\kappa}+\Delta t_{\mathrm{t}}} \\ & - \grave{s}_{j-(1/2),k+(1/2)}^{t_{n,\kappa}+\Delta t_{\mathrm{t}}} + \grave{s}_{j+(1/2),k-(1/2)}^{t_{n,\kappa}+\Delta t_{\mathrm{t}}} - \grave{s}_{j+(1/2),k+(1/2)}^{t_{n,\kappa}+\Delta t_{\mathrm{t}}}). \end{aligned} \tag{62}$$

5.1.1. Numerical derivatives

We now discuss our choice for the numerical derivatives (48), (49), (59) and (60). Consider z to be a generic grid function defined on a grid with nx versus ny cells ($nx \cdot ny = M$). In the numerical derivatives given below the MinMod$\{\cdot,\cdot\}$ is the usual limiter (see [33]),

$$\mathrm{MM}\{a,b\} \equiv \mathrm{MinMod}\{a,b\} = \tfrac{1}{2}[\mathrm{sgn}(a)+\mathrm{sgn}(b)]\cdot \mathrm{Min}(|a|,|b|), \tag{63}$$

where a and b are real numbers.

For the cells $3 \le j \le nx-2$ and $1 \le k \le ny$ in the x direction and $1 \le j \le nx$ and $3 \le k \le ny-2$ in the y direction we employ the UNO limiter [24] given by

$$z'_{j,k} = \mathrm{MM}\{\Delta z_{j-(1/2),k} + \tfrac{1}{2}\mathrm{MM}\{\Delta^2 z_{j-1,k}, \Delta^2 z_{j,k}\}, \Delta z_{j+(1/2),k} - \tfrac{1}{2}\mathrm{MM}\{\Delta^2 z_{j,k}, \Delta^2 z_{j+1,k}\}\}, \tag{64}$$

and

$$\grave{z}_{j,k} = \mathrm{MM}\{\Delta z_{j,k-(1/2)} + \tfrac{1}{2}\mathrm{MM}\{\Delta^2 z_{j,k-1}, \Delta^2 z_{j,k}\}, \Delta z_{j,k+(1/2)} - \tfrac{1}{2}\mathrm{MM}\{\Delta^2 z_{j,k}, \Delta^2 z_{j,k+1}\}\}, \tag{65}$$

respectively, where

$\Delta^2 z_{j,k} \equiv z_{j+1,k} - 2z_{j,k} + z_{j-1,k}$, $\Delta^2 z_{j,k} \equiv z_{j,k+1} - 2z_{j,k} + z_{j,k-1}$, $\Delta z_{j+\frac{1}{2},k} \equiv z_{j+1,k} - z_{j,k}$, and $\Delta z_{j,k+\frac{1}{2}} \equiv z_{j,k+1} - z_{j,k}$.

For the cells $j = 2, nx-1$ and $1 \le k \le ny$ in the x direction and $1 \le j \le nx$ and $k = 2, ny-1$ in the y we use,

$$z'_{j,k} = \mathrm{MM}\{\theta\,\mathrm{MM}\{\Delta z_{j+(1/2),k}, \Delta z_{j-(1/2),k}\}, \tfrac{1}{2}(\Delta z_{j+(1/2),k} + \Delta z_{j-(1/2),k})\}, \tag{66}$$

and

$$\grave{z}_{j,k} = \mathrm{MM}\{\theta\,\mathrm{MM}\{\Delta z_{j,k+(1/2)}, \Delta z_{j,k-(1/2)}\}, \tfrac{1}{2}(\Delta z_{j,k+(1/2)} + \Delta z_{j,k-(1/2)})\}. \tag{67}$$

Here $\theta \in (0.2)$ is a nonoscillatory limiter (see [28]). For our computations we use $\theta = 1.0$.

For the cells $j = 1, nx$ and $1 \le k \le ny$ in the x direction and $1 \le j \le nx$ and $k = 1, ny$ in the y we use,

$$z'_{j,k} = z_{j+1,k} - z_{j,k} \quad \text{and} \quad \grave{z}_{j,k} = z_{j,k+1} - z_{j,k}, \tag{68}$$

respectively.

We refer to [27,30] for information about nonoscillatory boundary treatments.

We remark that for the numerical approximation of the system (22)–(23) we employ a componentwise extension [33] of the scheme described above.

6. Numerical experiments

In our one and two-dimensional experiments we consider two Riemann problems, RP_1 and RP_2, whose left and right states are given by:

$$\mathrm{RP}_1 = \begin{cases} S_{\mathrm{w}}^{\mathrm{L}} = 0.613,\ S_{\mathrm{w}}^{\mathrm{R}} = 0.05 \\ S_{\mathrm{g}}^{\mathrm{L}} = 0.387,\ S_{\mathrm{g}}^{\mathrm{R}} = 0.15 \end{cases} \quad \text{and} \quad \mathrm{RP}_2 = \begin{cases} S_{\mathrm{w}}^{\mathrm{L}} = 0.721,\ S_{\mathrm{w}}^{\mathrm{R}} = 0.05 \\ S_{\mathrm{g}}^{\mathrm{L}} = 0.279,\ S_{\mathrm{g}}^{\mathrm{R}} = 0.15. \end{cases} \tag{69}$$

We work with the system of Eqs. (14)–(18) in dimensionless form.

We use the Leverett model [29] for capillary pressures given by

$$p_{\mathrm{wo}} = 5\epsilon(2 - S_{\mathrm{w}})(1 - S_{\mathrm{w}}) \quad \text{and} \quad p_{\mathrm{go}} = \epsilon(2 - S_{\mathrm{g}})(1 - S_{\mathrm{g}}), \tag{70}$$

where the coefficient ϵ controls the relative importance of capillary/dispersive and advective forces. We take $\epsilon = 1.0 \times 10^{-3}$ unless a different value is mentioned explicitly. The viscosities of the fluids are $\mu_{\mathrm{o}} = 1.0$, $\mu_{\mathrm{w}} = 0.5$, and $\mu_{\mathrm{g}} = 0.3$. We also adopt the model by Corey–Pope [11,15] which has been used extensively for phase relative permeabilities: $k_{\mathrm{w}} = S_{\mathrm{w}}^2$, $k_{\mathrm{o}} = S_{\mathrm{o}}^2$ and $k_{\mathrm{g}} = S_{\mathrm{g}}^2$. This model has the peculiarity that for a particular state in the interior of the saturation triangle the characteristic speeds of the hyperbolic system (22) coincide, or resonate. Such a state, whose location is determined by the fluid viscosities, is called an umbilic point [26]. It plays a central role in three-phase flow; in particular, its existence leads to the occurrence on nonclassical transitional shock waves in the solutions of the three-phase flow model. Crucial to calculating transitional shock waves is the correct modeling of capillarity (diffusive) effects [25].

For other models of three-phase flow used in petroleum engineering, such as certain models of Stone [39,17], the umbilic point is generally replaced by an elliptic region, in which the characteristic speeds are not real. In general, under reasonable physical assumptions about a model for immiscible three-phase flow, hyperbolic singularities such as umbilic points and elliptic regions are a necessary consequence of Buckley–Leverett behavior on each two-phase edge of the saturation triangle [38,32].

We remark that for the choice of parameters described above a transitional (intermediate) shock wave appears in the one-dimensional solution of RP_2. Such a wave is not present in the one-dimensional solution of RP_1.

6.1. One-dimensional results

Our one-dimensional solutions computed on a grid with 250 cells show very good agreement with the ones obtained on finer grids, and we note that our numerical solutions are in agreement with the semi-analytic results reported in [31].

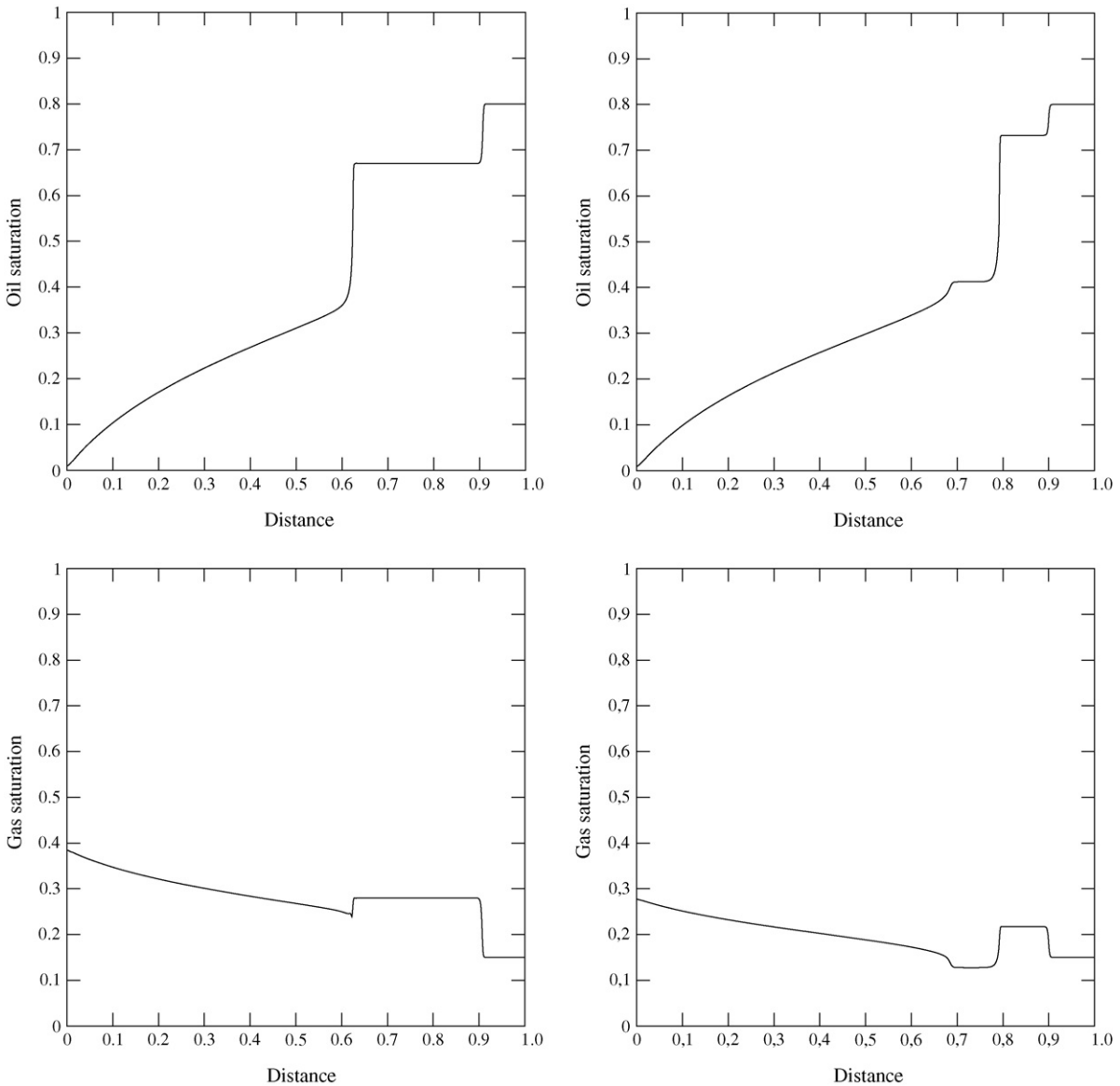

Fig. 2. From top to bottom profiles for oil and gas saturation are shown as a function of dimensionless distance. RP_1 on the left and RP_2 on the right; a transitional shock wave appears in RP_2.

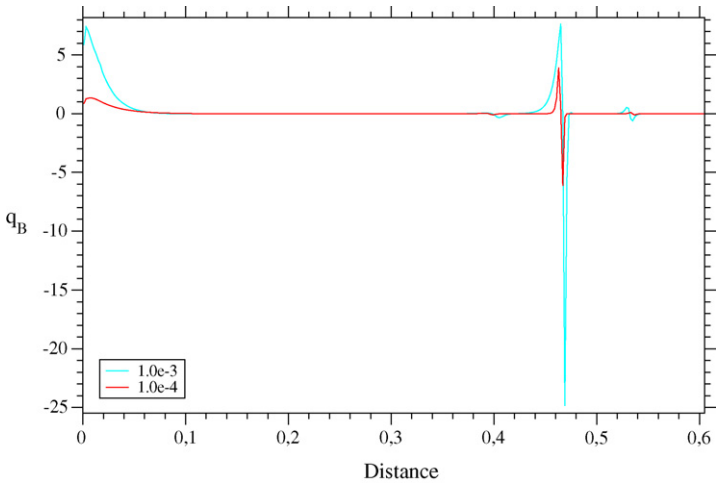

Fig. 3. The source term q_B is shown as a function of dimensionless distance for two values of the parameter ϵ: 1.0×10^{-3} (blue) and 1.0×10^{-4} (red).

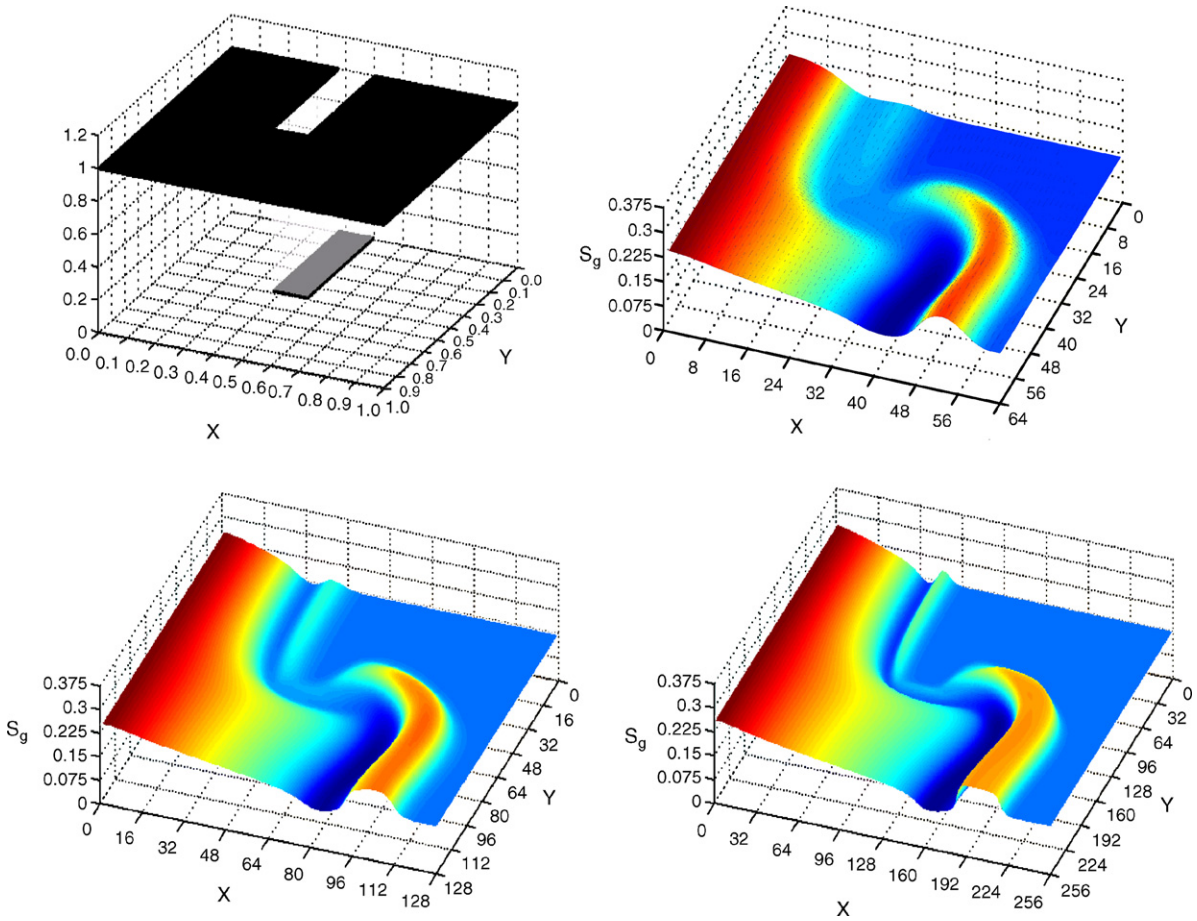

Fig. 4. Mesh refinement study for the RP_2 data in two spatial dimensions.

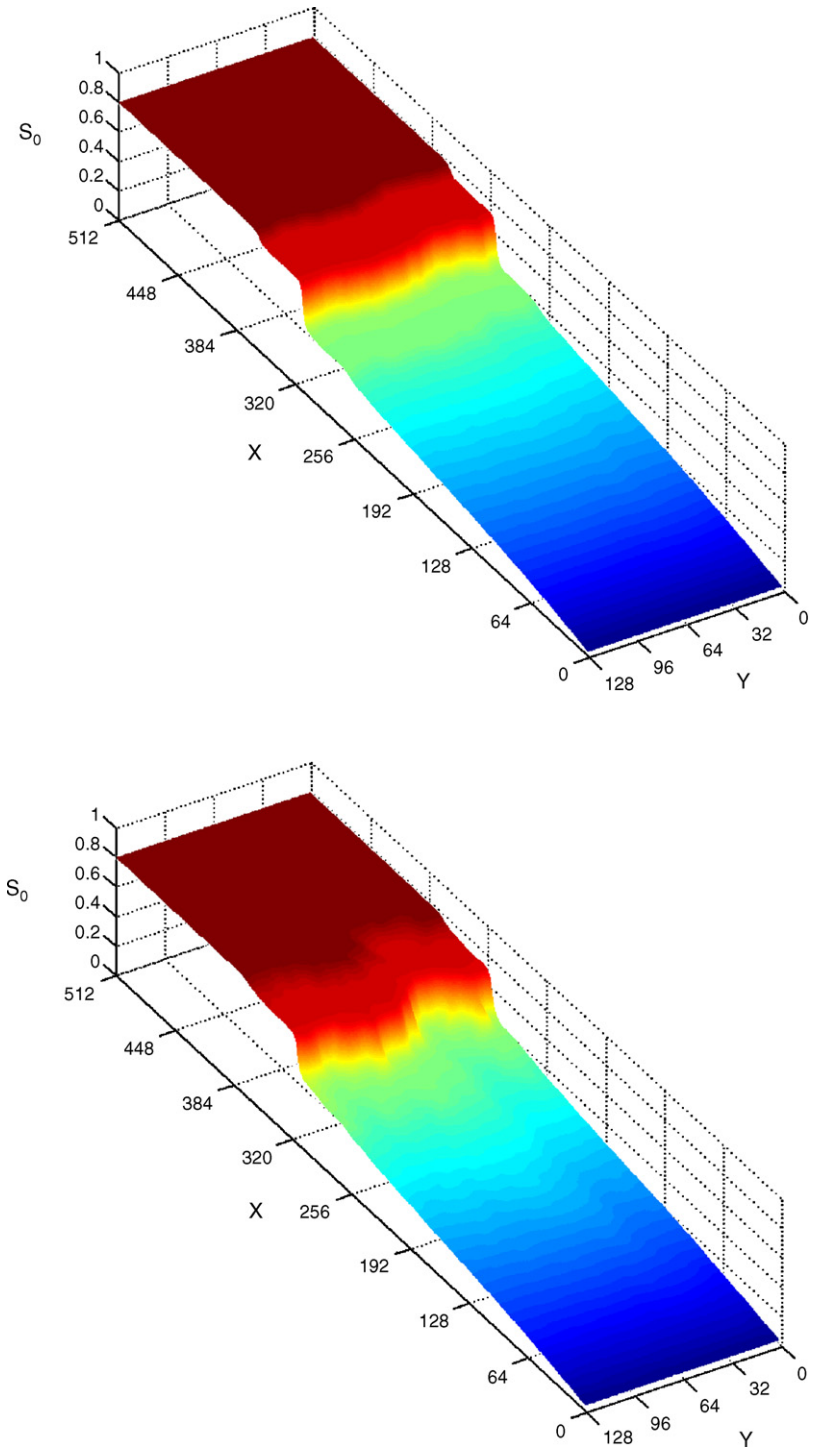

Fig. 5. Oil saturation surface plots for three-phase flow problems in 2D heterogeneous reservoirs; RP_2 data. From top to bottom are shown oil saturation surface plots with $C_v = 0.5$ and $C_v = 2.0$. Permeability fields with $\beta = \infty$ are considered. A transitional shock wave is simulated.

Fig. 2 shows from top to bottom saturation profiles for oil and gas as a function of dimensionless distance and time. The pictures on the left refer to RP_1 and the ones on the right refer to RP_2 (note the occurrence of the transitional wave).

Fig. 3 shows the source term (31) for two values of the parameter ϵ: 1.0×10^{-3} (blue) and 1.0×10^{-4} (red). We remark that the relation (32) is verified numerically; in fact, we use this identity as one criterion to stop the iterative scheme which solves for diffusive effects (described in Section 4.2).

6.2. Two-dimensional results

A numerical convergence study is performed for the permeability field displayed in the top left picture of Fig. 4; the remaining pictures in this figure show saturation surface plots for the gas phase.

A mixture (72.1% of water and 27.9% of gas) is injected at a constant rate of 0.2 pore volumes every year along the boundary, $x = 0$ and $y \in [0, 1]$, of the computational region. The initial conditions for the system is given by $S_w^R = 0.05$ and $S_g^R = 0.15$; these data correspond to RP_2. Two values are specified for the permeability field in the computational region: 0.01 in a rectangle which touches the top boundary and 1.0 elsewhere. The computational grids used were 64 versus 64 (top right picture), 128 versus 128 (bottom left picture) and 256 versus 256 (bottom right picture). Clearly the 64 versus 64 grid can resolve the low permeability region and captures the transitional (intermediate) wave; as the grid is refined the jumps in the numerical solution get sharper, indicating numerical convergence of our new procedure. Note that spurious oscillations do not occur in the numerical solutions.

We reiterate that transitional waves have a strong dependency upon the physical diffusion being modeled (see [31] and references therein); note that rock heterogeneity introduces variability in the diffusion term of Eqs. (14a) and (14b). The goal of the numerical experiments reported below is the investigation of the occurrence of transitional waves in two-dimensional, multiscale heterogeneous problems. As mentioned above such waves have been observed only in one-dimensional problems.

As a model for multi-length scale rock heterogeneity we consider scalar, log-normal permeability fields, so that $\xi(\mathbf{x}) = \log K(\mathbf{x})$ is Gaussian and its distribution is determined by its mean and covariance function. We assume the distribution is stationary, isotropic and fractal (self-similar). Thus, the mean is an absolute constant and the covariance

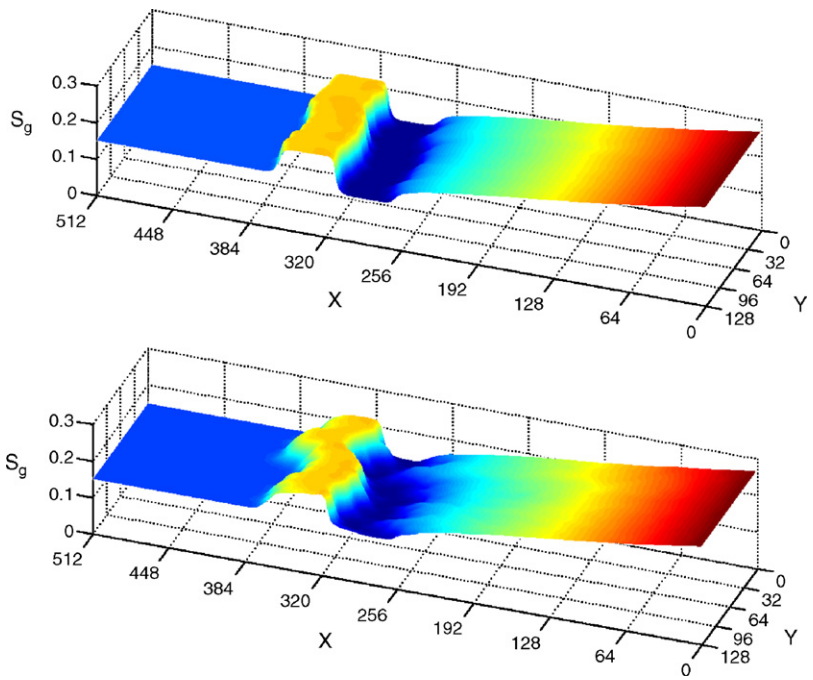

Fig. 6. Gas saturation surface plots for three-phase flow problems in 2D heterogeneous reservoirs; RP_2 data. From top to bottom are shown gas saturation surface plots with $C_v = 0.5$ and $C_v = 2.0$. Permeability fields with $\beta = \infty$ are considered.

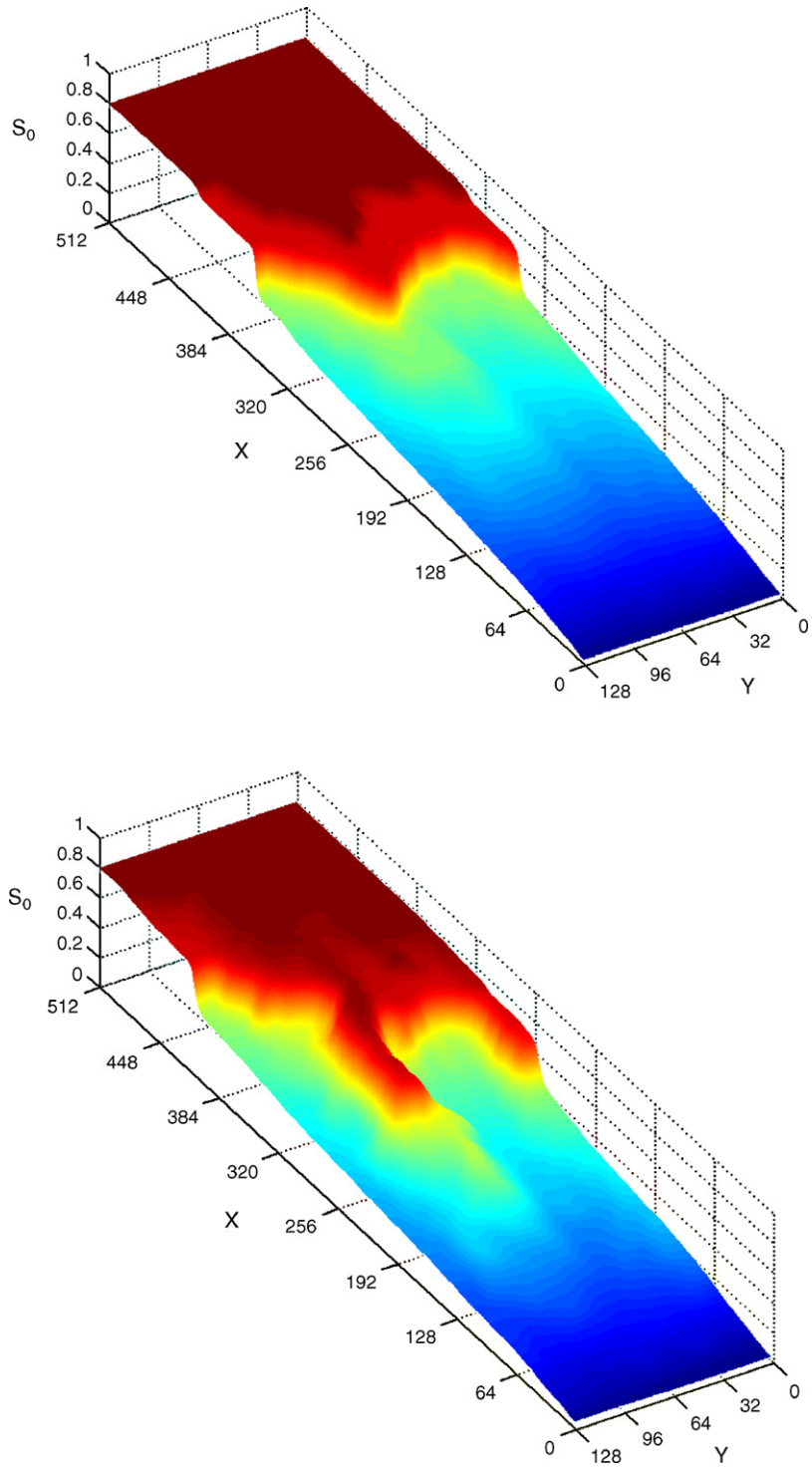

Fig. 7. Oil saturation surface plots for three-phase flow problems in 2D heterogeneous reservoirs; RP_2 data. From top to bottom are shown oil saturation surface plots for $C_v = 0.5$ and $C_v = 2.0$. Permeability fields with $\beta = 0.5$ are considered.

is given by a power law:

$$\mathrm{Cov}(\mathbf{x}, \mathbf{y}) = |\mathbf{x} - \mathbf{y}|^{-\beta}, \quad \beta > 0. \tag{71}$$

The scaling exponent β controls the nature of multiscale heterogeneity: as it increases, the heterogeneities concentrated in the larger length scales are emphasized and the field becomes more regular (locally). In our numerical studies we also consider log-normal, statistically independent random fields. We refer to such fields by $\beta = \infty$. See [19] for a discussion of the numerical construction of fractal fields.

The spatially variable permeability fields are defined on 512×128 grids with two values for the coefficiente of variation C_v ((standard deviation)/mean): 0.5 and 2.0. C_v is used as a dimensionless measure of the heterogeneity of the permeability field. The computed fluid flows are defined in a bounded two-dimensional reservoir $\Omega = [0, X] \times [0, Y]$ with aspect ratio $X/Y = 4$, discretized by an uniform grid of 512×128 cells. Again, a mixture (72.1% of water and 27.9% of gas) is injected at a constant rate of 0.2 pore volumes every year along the boundary, $x = 0$ and $y \in [0, Y]$, of the computational region. The initial conditions for the system correspond to RP_2.

In Figs. 5 and 6 we show saturation surface plots for oil and gas, respectively, displayed as a function of position. Uncorrelated Gaussian field ($\beta = \infty$) permeability fields were considered; these figures refer permeability fields with $C_v = 0.5$ and 2.0, from top to bottom. Note in these figures that for both large and small strength heterogeneities transitional shock waves were properly simulated.

Correlated Gaussian ($\beta = 0.5$) permeability fields were used in the simulations reported in Figs. 7 and 8. In these figures the values $C_v = 0.5$ and 2.0 were considered (from top to bottom) and saturation surface plots are shown for oil (Fig. 7) and gas Fig. 8. Note that for $C_v = 0.5$ and long-range rock correlations transitional shock waves were properly simulated. However, for long-range correlations and stronger heterogeneity ($C_v = 2.0$) the separate identity of the transitional shock and its precursor Buckley–Leverett shock seems to be lost.

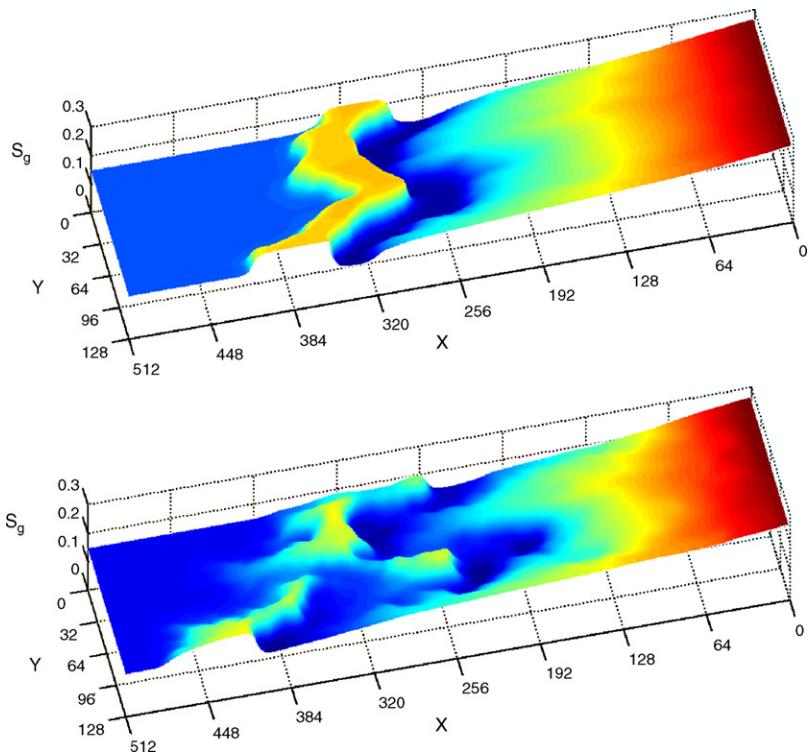

Fig. 8. Gas saturation surface plots for three-phase flow problems in 2D heterogeneous reservoirs; RP_2 data. From top to bottom are shown gas saturation surface plots for $C_v = 0.5$ and $C_v = 2.0$. Permeability fields with $\beta = 0.5$ are considered.

7. Concluding remarks

A new simulator intended for the numerical solution of three-phase, two-dimensional immiscible displacement problems in heterogeneous reservoirs has been described in detail. The numerical tests performed indicate that the simulator is accurate. The new simulator was used to extend theoretical results for one-dimensional flows by providing numerical evidence of the existence of transitional waves in two-dimensional flows.

A two-level fractional-step numerical technique is introduced for the numerical solution of the problem at hand. The nonlinear advection, diffusion and pressure–velocity problems that result from the splitting are approximated sequentially by a nonoscillatory, second-order, conservative central difference scheme (for advection) and locally conservative mixed finite elements (for diffusion and pressure–velocity).

The numerical simulation of the full two-dimensional coupled set of pressure–velocity-saturation Eqs. (14)–(17) shows that the heterogeneity has an important effect on the transitional shock front. We recall that this shock is related to the loss of strict hyperbolicity inherent in the pure 1D system of conservation laws for the saturations and that this shock is very sensitive to diffusive effects. Our numerical simulations indicates that, the transitional shock persists under the presence of heterogeneities and is accurately captured by our simulator, as shown by comparisons with reliable 1D simulations and calculations for homogeneous media [31]. Moreover, the transitional shock is stable under the excitations imposed by short-range or weak (small C_v) heterogeneities. On the other hand, for strong, long-range excitations the separate identity of the transitional wave and its precursor Buckley–Leverett shock seems to be lost.

As a first step in the investigation of the scale-up problem for three-phase flow the authors are currently investigating the stability (with respect to viscous fingering) of transitional waves in heterogeneous formations; stable transitional waves could improve drastically oil production. The upscaled behavior of two-phase flow in heterogeneous media is strongly dependent on flow regime [20,4,21]. The preliminary results of the current investigation seem to indicate that scale-up would have to be done wave by wave, perhaps precluding the existence of effective upscaled partial differential equations for three-phase flow in heterogeneous porous media.

Acknowledgments

E.A. thanks CAPES (IPRJ/UERJ) for a Ph.D. fellowship and the organizers of the 2004 PASI meeting for a fellowship which allowed him to attend this event. F.P. was supported in part through grants CNPq/CTPetro 501886/03-6, CNPq/CTPetro 70216/03-4, CNPq/Universal 470216/03-4, CNPq/FAPERJ PRONEX (2003–2006). D.M., F.F. and F.P. wish to acknowledge the support from the CNPq and the NSF for an international collaborative research project on improved oil recovery through scale up for multiphase flow.

References

[1] E. Abreu, Numerical simulation of three-phase water–oil–gas flows in petroleum reservoirs, M.Sc Thesis, IPRJ/UERJ, Brazil, 2003. (in Portuguese, available at http://www.labtran.iprj.uerj.br/Orientacoes.html).
[2] E. Abreu, F. Furtado, F. Pereira, On the numerical simulation of three-phase reservoir transport problems, Transport Theory Stat. Phys. 33 (5–7) (2004) 503–526.
[3] D.N. Arnold, F. Brezzi, Mixed and nonconforming finite element methods: implementation, postprocessing and error estimates, R.A.I.R.O. Modélisation Mathématique et Analyse Numérique 19 (1985) 7–32.
[4] V. Artus, F. Furtado, B. Noetinger, F. Pereira, Stochastic analysis of two-phase immiscible flow in stratified porous media, Computat. Appl. Math. 23 (2–3) (2004) 153–172.
[5] A. Azevedo, D. Marchesin, B.J. Plohr, K. Zumbrun, Capillary instability in models for three-phase flow, Zeit. Angew. Math. Phys. 53 (5) (2002) 713–746.
[6] M. Aziz, A. Settari, Petroleum Reservoir Simulation, Elsevier Applied Science, New York, 1990.
[7] I. Berre, H.K. Dahle, K.H. Karlson, H.F. Nordhaug, A streamline front tracking method for two- and three-phase flow including capillary forces, Proceedings of an AMS-IMS-SIAM, Joint Summer Research Conference on Fluid Flow and Transport in Porous Media: Mathematical and Numerical Treatment, vol. 295, Mount Holyoke College, South Hadley, Massachusetts, June 17–21, 2002, pp. 49–61.
[8] A. Bertozzi, A. Munch, M. Shearer, Undercompressive shocks in thin flim, Phys. D 134 (1990) 431–464.
[9] Z. Chen, Formulations and numerical methods of the black oil model in porous media, SIAM J. Numer. Anal. 38 (2) (2000) 489–514.
[10] Z. Chen, R.E. Ewing, Fully-discrete finite element analysis of multiphase flow in ground-water hydrology, SIAM J. Numer. Anal. 34 (1997) 2228–2253.
[11] A. Corey, C. Rathjens, J. Henderson, M. Wyllie, Three-phase relative permeability, Trans. AIME 207 (1956) 349–351.

[12] J. Douglas, R.E. Ewing Jr., M.F. Wheeler, The approximation of the pressure by a mixed method in the simulation of miscible displacement, R.A.I.R.O., Anal. Numér. 17 (1983) 17–33.
[13] J. Douglas Jr., F. Furtado, F. Pereira, On the numerical simulation of waterflooding of heterogeneous petroleum reservoirs, Comput. Geosci. 1 (1997) 155–190.
[14] J. Douglas Jr., P.J. Paes Leme, J.E. Roberts, J. Wang, A parallel iterative procedure applicable to the approximate solution of second order partial differential equations by mixed finite element methods, Numer. Math. 65 (1993) 95–108.
[15] D.E. Dria, G.A. Pope, K. Sepehrnoori, Three-phase gas/oil/brine relative permeabilities measured under CO_2 flooding conditions, Soc. Petr. Engrg. SPE 20184 (1993) 143–150.
[16] A. Falls, W. Schulte, Theory of three-component, three-phase displacement in porous media, SPE Reserv. Eng. 7 (1992) 377–384.
[17] F. Fayers, J. Matthews, Evaluation of normalized Stone's method for estimating three-phase relative permeability, Soc. Petr. Engrg. J. 24 (1984) 225–232.
[19] F. Furtado, J. Glimm, B. Lindquist, F. Pereira, Multi-length scale calculations of mixing length growth in tracer floods, F. Kovarik (ed.), Proceedings of the Emerging Technologies Conference, Houston, TX, 1990.
[20] F. Furtado, F. Pereira, Crossover from nonlinearity controlled to heterogeneity controlled mixing in two-phase porous media flows, Comput. Geosci. 7 (2003) 115–135.
[21] J. Glimm, H. Kim, D. Sharp, T. Wallstrom, A stochastic analysis of the scale up problem for flow in porous medium, Comput. Appl. Math. 17 (1998) 67–79.
[22] R. Guzmán, F. Fayers, Mathematical properties of three-phase flow equations, SPE J., 2 (1997) 291–300 (SPE 35154).
[23] R. Guzmán, F. Fayers, Solutions to the three-phase flow Buckley-Leverett problem, SPE J., 2 (1997) 301–311 (SPE 35156).
[24] A. Harten, S. Osher, Uniformly high order accurate non-oscillatory scheme I, SINUM 24 (1987) 279.
[25] E. Isaacson, D. Marchesin, B. Plohr, Transitional waves for conservation laws, SIAM J. Math. Anal. 21 (1990) 837–866.
[26] E. Isaacson, D. Marchesin, B. Plohr, J.B. Temple, Multiphase flow models with singular Riemann problems, Comput. Appl. Math. 11 (1992) 147–166.
[27] G.S. Jiang, D. Levy, C.T. Lin, S. Osher, E. Tadmor, High-resolution non-oscillatory central schemes with non-staggered grids for hyperbolic conservation laws, SIAM J. Numer. Anal. 35 (1998) 2147–2168.
[28] R. Kupferman, E. Tadmor, A fast high resolution second order central scheme for incompressible flows, Proc. Natl. Acad. Sci. U.S.A. 94 (May (10)) (1997) 4848–4852.
[29] M.C. Leverett, W.B. Lewis, Steady flow of gas-oil-water mixtures through unconsolidated sands, Trans. SPE AIME 142 (1941) 107–16.
[30] D. Levy, E. Tadmor, Non-oscillatory boundary treatment for staggered central scheme, UCLACAM, 1998. (Available at http://www.cscamm.umd.edu/∼tadmor/pub/general.htm).
[31] D. Marchesin, B.J. Plohr, Wave structure in WAG recovery, SPEJ 6 (2) (1999/2001) 209–219 (SPE 56480).
[32] H. Medeiros, Stable hyperbolic singularities for three phase flow models in oil reservoir simulation, Acta Appl. Math. 28 (1992) 135–159.
[33] N. Nessyahu, E. Tadmor, Non-oscillatory central differencing for hyperbolic conservation laws, J. Comput. Phys. (1990) 408–463.
[34] D.W. Peaceman, Fundamentals of Numerical Reservoir Simulation, Elsevier, Amsterdam, 1977.
[35] P-A. Raviart, J.M. Thomas, A mixed finite element method for second order elliptic problems, in: I. Galligani, E. Magenes (eds.), Mathematical Aspects of the Finite Element Method, Lecture Notes in Mathematics, vol. 606, Springer-Verlag, Berlin/New York, 1977, pp. 292–315.
[36] A.E. Scheidegger, The Physics of Flow Through Porous Media, University of Toronto Press, 1957.
[37] W. Schulte, A. Falls, Features of three-component, three-phase displacement in porous media, SPE Reserv. Eng. 7 (1992) 426–432.
[38] M. Shearer, Loss of strict hyperbolicity of the Buckley–Leverett equations for three-phase flow in a porous medium, IMA Vol. Math. Appl. 11 (1988) 263–283.
[39] H. Stone, Probability model for estimating three-phase relative permeability, J. Petr. Tech. 22 (1970) 214–218.